Applied Physics A (2021) 127:573
https://doi.org/10.1007/s00339-021-04722-3

Applied Physics A
Materials Science & Processing

The electric field gradient as a signature of the binding and the local structure of adatoms on graphene

A. S. Fenta[1,2,3] · C. O. Amorim[2] · J. N. Gonçalves[2] · N. Fortunato[2] · M. B. Barbosa[4,5,6] · S. Cottenier[7,8] · J. G. Correia[3,9] · L. M. C. Pereira[1] · V. S. Amaral[2]

Received: 7 April 2021 / Accepted: 22 June 2021 / Published online: 2 July 2021

Abstract
We examined the interaction between adatoms and graphene for Ag, Cd, In and Hg by density functional theory. We establish a relation between the binding energy and the electric-field gradient tensor (EFG) for each atom, which indicates that hyperfine interactions can be used to probe the binding and stability of adatoms on graphene. The EFG is also shown to be a fingerprint for the local configuration, even at the sub-Angstrom scale. This work demonstrates how suitable hyperfine methods, such as perturbed angular correlation spectroscopy, can be used to experimentally unravel details of atomic adsorption on graphene, and by extension on two-dimensional materials in general.

Keywords Graphene · Adatoms · Electric field gradient · Binding energy · Hyperfine interactions

1 Introduction

Graphene properties are intimately dependent on the two-dimensionality (2D) of its structure [1–3]. Being a single atomic layer, the adsorption of guest atoms (adatoms) or molecules (admolecules) has a strong effect on the properties of graphene. Adatoms and admolecules are therefore a promising way to modify the properties of graphene and engineer a specific functionality that can be used in technological applications. Several studies have reported that structural, electronic and magnetic properties of graphene can be manipulated using adsorption of atoms, individually or organized in clusters [4–7]. Understanding the adsorption process of certain species on graphene requires studying their position stability relative to the underlying carbon honeycomb lattice [8].

Techniques such as scanning tunnelling microscopy (STM) [9] and transmission electron microscopy (TEM) [10] have been extensively used to characterize the topographic and local electronic structure of graphene–adsorbent systems. Here, we investigate to what extent the electric field gradient (EFG) can be used to probe the adatom–graphene interaction, adsorption stability, and local atomic configuration, owing to the high sensitivity of the EFG to changes

✉ C. O. Amorim
amorim5@ua.pt

1 Instituut voor Kern-en Stralingsfysica, KU Leuven, Celestijnenlaan 200 D, 3001 Leuven, Belgium

2 Physics Department and CICECO, University of Aveiro, 3810-193 Aveiro, Portugal

3 CERN, 1211 Geneva, Switzerland

4 IFIMUP and IN-Institute of Nanoscience and Nanotechnology, Departamento de Física e Astronomia da Faculdade de Ciências da Universidade do Porto, Rua do Campo Alegre 687, 4169-007 Porto, Portugal

5 Department of Physics, Faculty of Science, National University of Singapore, 2 Science Drive 3, Singapore 117542, Singapore

6 Centre for Advanced 2D Materials, National University of Singapore, 6 Science Drive 2, Singapore 117546, Singapore

7 Center for Molecular Modeling, Ghent University, 9052 Zwijnaarde, Belgium

8 Department of Electrical Energy, Metals, Mechanical Constructions and Systems, Ghent University, 9052 Zwijnaarde, Belgium

9 Instituto Superior Técnico, Campus Tecnológico e Nuclear, EN10, C2TN, 2695-066 Bobadela, Portugal

in the local charge distribution. The EFG can be measured experimentally via its interaction with the nuclear electric quadrupole moment of a suitable probe atom, using techniques such as nuclear quadrupole resonance (NQR), Mössbauer spectroscopy (MS) or perturbed angular correlation (PAC) technique. Such measurements are particularly sensitive to changes induced by lattice distortions, such as host impurities or defects [11, 12] because they modify the local electrostatic potential, thus creating its own characteristic EFG. Therefore, the process of adsorption, spatial configuration and the stability of a certain adatom on graphene can be directly related to the experimentally determined EFG.

The EFG is a traceless symmetric rank 2 tensor, defined as:

$$V_{ij} = \Phi_{ij} - \frac{1}{3} Tr(\Phi) \tag{1}$$

where $\Phi(\vec{r})$ is the electric potential due to the electron cloud at the nucleus position ($\vec{r} = 0$) and Φ_{ij} is defined as $\Phi_{ij} = \frac{\partial^2 \Phi(\vec{r})}{\partial x_i \partial x_j}$ [11, 13]. The tensor is symmetric due to the commutation of the second partial derivatives of the electrostatic potential $\Phi(\vec{r})$, and it is also traceless at the probe site by definition, since the nucleus is approximated to a point charge from the point of view of the external electronic charge. The axis system can be defined in a way that the EFG tensor representation has only three non-vanishing diagonal components defined as $|V_{zz}| \geq |V_{yy}| \geq |V_{xx}|$. For simplicity, it is common to characterize the EFG tensor by its main component V_{zz} and the axial asymmetry parameter, η, defined by:

$$\eta = \frac{V_{yy} - V_{xx}}{V_{zz}} \tag{2}$$

taking into account that the three remaining degrees of freedom are characterized by the Euler angles that correlate the principal axis system where the EFG is diagonal with the axis system where the laboratory is defined.

A precise calculation of the entire electronic configuration of graphene and the adatoms can be performed using density functional theory (DFT). DFT calculations have assumed an important role in experimental data interpretation of the EFGs measured with hyperfine techniques [14–16].

This paper presents a set of DFT studies of electronic structure and EFG tensor for selected adatom elements on graphene: Ag, Cd, In and Hg. In our previous work [17], we have shown that it is possible to distinguish dilute Hg configurations from monolayer configurations, based on experimentally measured EFG values. Here, we show that for other elements, under adequate conditions, it is possible to obtain much more detailed insight into the local atomic configuration (even distinguishing the adsorption site in the dilute regime), as well as on the structural stability and charge distribution around a probe adatom. We chose the Ag, Cd, In and Hg adatoms since they are already widely studied using PAC spectroscopy due to the availability of suitable isotopes (with favourable and well-established decay schemes and nuclear moments). These calculations provide insight on the stability of various adsorption configurations and its relation with the EFG tensor. In particular, it sets the basis for a new experimental approach that is currently being developed at the ISOLDE facility at CERN [18], using the ASPIC setup (Apparatus for Surface Physics and Interfaces at CERN) [19], where a multitude of radioactive isotopes can be deposited and measured in situ with PAC spectroscopy.

2 Computational methods

The DFT calculations were performed using WIEN2K [20], which implements the linearized augmented plane wave (LAPW) method [21–23]. This method divides space into non-overlapping spheres described by spherical harmonics and the interstitial region, described by plane waves. It is an all-electron code (employing the full charge distribution of all electrons) and for this reason particularly suited to calculate hyperfine parameters. The muffin-tin radii were set to 1.29 and 1.70 atomic units, for the carbon atoms and for the adatoms, respectively. The number of plane waves is set by the parameter $R_{mt} \times K_{\max} = 5.5$, where $R_{mt} = 1.29$ a.u. (the radius of the smallest sphere).

The nominal concentration of the adatoms with respect to the number of carbon atoms in the unit cell was $\theta = 1/18$, corresponding to a 3×3 (C-hexagon) supercell, with a grid of $10 \times 10 \times 1k$-points. This nominal concentration ensures that there is virtually no interaction between adatoms to compete with the interaction with the graphene layer [17]. Three sets of calculations for each adatom were performed for the different adsorption sites with the highest symmetry (Fig. 1): the hollow (H) site, the top (T) site and the bridge (B) site. An additional configuration was also considered in the calculations: an hexagonal monolayer with the atoms in a sequence of H-T-T sites (therefore designated here as HTT configuration), with a concentration of $\theta = 3/8$ with respect to C atoms, with an in plane interatomic distance (2.84Å) which is comparable to solid Ag, Cd, In and Hg, in bulk. The HTT configuration is equivalent to a (111) plane of a cubic lattice, which is a typical interfacial structure between graphene on various <111>-oriented metal substrates (e.g. Al, Au, Pd and Pt) [24]. A vacuum spacing of at least 16 Å between adjacent layers is used, to minimize interlayer interactions [17].

The calculations did not consider spin polarization. The generalized gradient approximation (GGA-PBE) [25] with van der Waals correction (DFT-D3) [26] for the exchange correlation functional was used. The experimental lattice parameter $a = b = 2.46$Å, which is close to the optimized parameters with GGA (2.47 Å) for undoped graphene, was adopted [17].

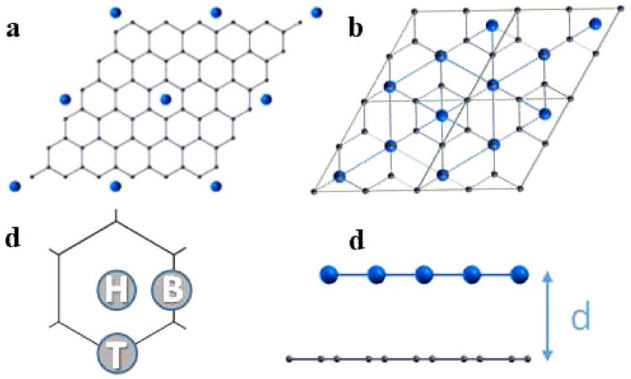

Fig. 1 Atomic configurations considered in the calculations: **a** 3×3 supercell for adatoms at the hollow site (H) on graphene, corresponding to a nominal concentration of $\theta = 1/18$ with respect to the number of carbon atoms; **b** the monolayer in a *HTT* configuration, with nominal concentration of $\theta = 3/8$; **c** the three high-symmetry positions on graphene, i.e. the hollow (H) site above the centre of the hexagon, the top (T) site on top of the C atoms, and the bridge (B) site above the middle of the C–C bonds; **d** graphene–adatom distance d

3 Results

We start by analysing the isolated adatom regime ($\theta = 1/18$), for the different high-symmetry positions (H, T, B). Figure 2 shows the adsorption energy curves of the graphene–adatom system, as a function of graphene–adatom distance d for Ag, Cd, In and Hg. The adatom stability on graphene is related to the adsorption energy (E_{ads}) which can be defined as:

$$E_{ads} = E_{G+adatom} - E_G - E_{adatom} \quad (3)$$

where $E_{G+adatom}$ is the energy of the system graphene plus adatom and E_G and E_{adatom} are the energy of graphene and the energy of the adatom, respectively. Larger absolute values of the adsorption energy correspond to stronger binding of the adatom to the surface of graphene. The binding energy (E_b) is defined as the absolute value of the minimum of the adsorption energy at a corresponding equilibrium distance (d_{eq}). Each adatom element (Ag, Cd, In and Hg) presents qualitatively similar shapes of the adsorption energy curve for the various high-symmetry sites (H, T, and B). However, both E_b and d_{eq} depend on the adatom element and adsorption site (Table 1). Apart from the Ag case, for which the binding energy reaches its highest value for the T-site (274 MeV), all the other adatoms have their highest binding energy at the H-site. Among the elements studied here, in the dilute regime ($\theta = 1/18$), we can conclude that In has the highest binding energy (666 MeV), and Hg the lowest (186 MeV). Also, with increasing binding energy, the corresponding graphene–adatom distance tends to decrease and therefore In stabilizes closer to the surface of graphene ($d_{eq} = 2.63$ Å) compared to Hg ($d_{eq} = 3.45$ Å).

Next, we compare the stability of the isolated adatoms ($\theta = 1/18$) to the HTT monolayer configuration ($\theta = 3/8$). Figure 3 displays the adsorption energy per adatom as a function of graphene–adatom distance, for Ag, Cd, In and

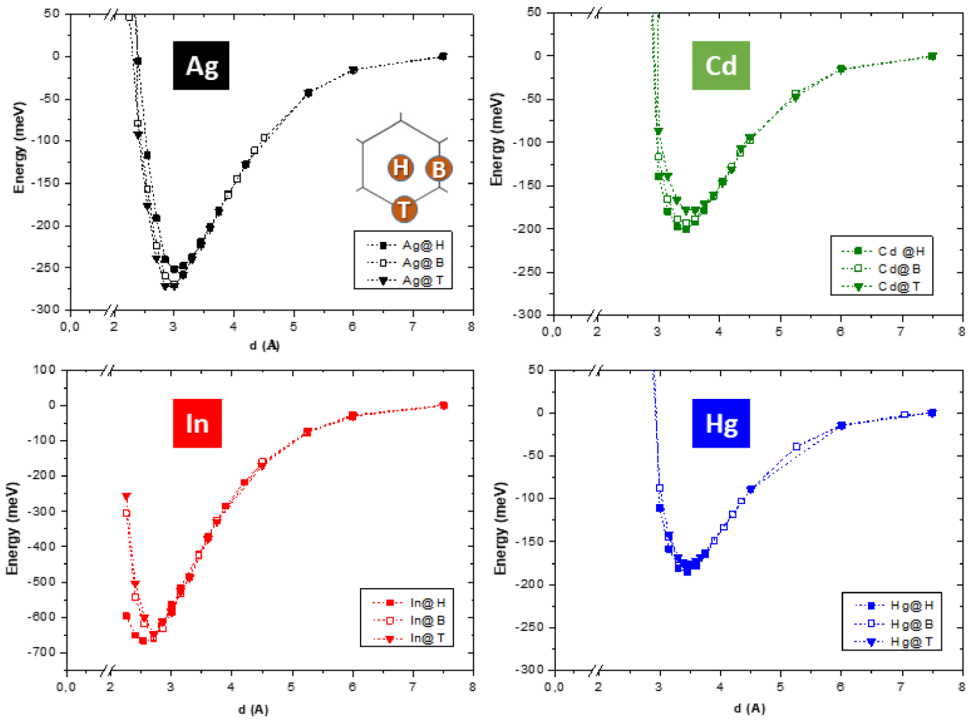

Fig. 2 Adsorption energy of the graphene–adatom system as a function of the distance (d) between graphene and the adatom for the three high-symmetry positions (H, B and T), for Ag, Cd, In and Hg, for a nominal concentration of $\theta = 1/18$

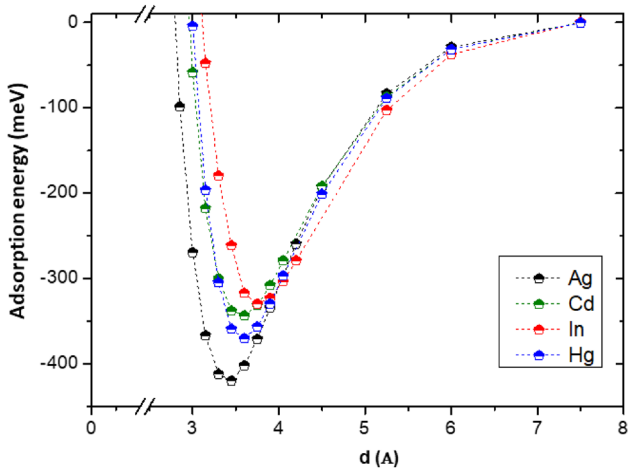

Fig. 3 Adsorption energy per adatom of the HTT configuration ($\theta = 3/8$) as a function of distance, d, for Ag, Cd, In and Hg

Hg in a HTT configuration. The respective binding energies are also compiled in Table 1. When the adatoms assume the HTT configuration on graphene, Ag has the largest binding energy (420 MeV) in contrast to In, with the lowest binding energy (330 MeV). For all the studied elements, the isolated adatom regime is predicted to have the highest binding energy per adatom (thus more stable) when compared to the HTT monolayer configuration.

In addition to the adsorption energies discussed above, for each configuration, we calculated the respective EFG parameters (V_{zz} and η). Since, only the isolated configuration on B sites, which is never the most stable position, exhibits a non-vanishing η value, we will solely focus on the V_{zz} parameter.[1]

The first key observation is that different configurations are associated with different values of V_{zz} (Table 1). In particular, the V_{zz} value is always significantly larger for the HTT configuration, compared to the stable isolated site.

Before discussing what kind of information can be experimentally assessed based on measurements of the EFG parameters, we first comment on the observed dependence of the V_{zz} on the distance d between the adatom and the graphene layer in the most stable position of the dilute regime ($\theta = 1/18$). In Fig. 4, the absorption energy and the V_{zz} (for each adatom element in the respective stable site, i.e. H or T) is plotted as a function of distance d (in $\sim$ 10 pm steps) in the vicinity of the equilibrium position d_{eq}.

Figure 4 shows that the sensitivity of V_{zz} to changes in d ($\Delta V_{zz}/\Delta d$) varies significantly among the different elements. Indium, which among the considered elements exhibits the highest binding energy and V_{zz} (25.0 V Å^{-2}), also shows the largest EFG sensitivity ($\Delta V_{zz}/\Delta d = 2.50$ V Å^{-2}/pm). To further analyse the trend across the different elements, let us define a relative variation, i.e. dividing $\Delta V_{zz}/\Delta d$ by the absolute value of the V_{zz} at the equilibrium distance (V_{zz}^{eq}), and expressing it as a percentage $|\ (\Delta V_{zz}/\Delta d)/V_{zz}^{eq}\ | \times 100\%$. These values (1.9%, 2.1%, 2.8% and 10% per pm, for Hg, Cd, Ag and In, respectively) are plotted in Fig. 5 as a function of the calculated binding energy (E_b).

Figure 5 shows that, for the most stable position of the dilute adatom regime ($\theta = 1/18$), there is a monotonous increase of EFG sensitivity with increasing E_b. This follows a similar trend to the absolute value of V_{zz} as a function of E_b, hence being correlated with the strength of the graphene–adatom binding in the isolated adatom regime . This relation can be understood based on the fact that the binding and the EFG have a common origin: orbital overlap (charge sharing) between the adatom and the graphene layer.

In order to gain further insight into how the binding (i.e. the electronic density distribution) is related to the EFG, we analysed the contributions to EFG from the orbitals involved in the binding (for each adatom element in its equilibrium position). The EFG inside the spheres can be analysed by separating the atomic-like functions into contributions corresponding to *Gaunt* numbers with different pairs of angular orbital momentum numbers [11]: *p–p*, *d–d* (*s–d* and *p–f*), which may be interpreted as electrons from the corresponding orbitals contributing to the EFG. For all the cases, the most significant contribution to the V_{zz} comes from *p–p* orbitals. The large difference between the most (In) and least (Cd) sensitive element, in terms of V_{zz}, results from the different amounts of *p*-orbital superposition.

To further illustrate the relation between the binding and the EFG, Fig. 6 shows the charge distribution and the charge isolines in the adatom–graphene system, from which the degree of charge sharing can be inferred. The highly symmetric charge distribution, with circular isolines of the outer electronic shells of the adatoms for the case of Cd and Hg (*d* orbitals fully-filled), leads to low V_{zz} values (-2.4 V/Å^2 and -6.6 V/Å^2, respectively). On the other hand, the higher V_{zz} values observed for In and Ag (25.0 V/Å^2 and -12.5 V/Å^2, respectively), are a consequence of the non-spherical charge distribution around the adatom (with *s* and *p* incomplete orbitals for In and Ag, respectively), caused by the strong interaction with the graphene lattice.

In other words, stronger charge sharing implies a stronger binding and more pronounced asymmetry of the outer electron shells along the binding direction, which in turn tends to produce a larger V_{zz} and a stronger sensitivity of V_{zz} to variations in d (since an increasing d is associated with a decrease in charge sharing). This notion is further supported by the fact that the same trend is not observed for the monolayer (HTT) regime, since there the EFG is

[1] For H and T sites η must necessarily be zero, since the z-axis is a threefold rotation axis.

Table 1 High-symmetry positions, binding energy (E_b) and corresponding distance (d_{eq}), EFG parameters (V_{zz} and η), stable isolated site (i.e. site with highest binding energy in the isolated configuration) meta-stable position (i.e. site with the second highest binding energy in the isolated configuration) and respective energy barrier for hopping between stable sites (ΔE_{hop}, i.e. energy difference between stable and meta-stable sites), for isolated adatoms ($\theta = 1/18$) and the HTT configuration ($\theta = 3/18$), for adsorbed Ag, Cd, In and Hg on graphene

θ	Concentration	Position	E_b (meV)	d_{eq} (Å)	V_{zz} (V/Å^2)	η	Stable isolated site	Meta-stable isolated site	ΔE_{hop} (meV)
Ag	1/18	H	252	3.10	− 0.7	0.00			
	1/18	T	**274**	**2**.90	− **12.5**	**0**.00	**T**	**B**	5
	1/18	B	269	3.00	1.0	0.24			
	3/8	HTT	140	3.45	65.10	0.00			
Cd	1/18	H	**201**	**3**.43	− **2.4**	**0**.00			
	1/18	T	181	3.60	− 0.30	0.00	**H**	**B**	7
	1/18	B	194	3.44	− 0.49	0.36			
	3/8	HTT	115	3.60	227.10	0.00			
In	1/18	H	**666**	**2**.63	**25.0**	**0**.00			
	1/18	T	645	2.73	− 1.6	0.00	**H**	**B**	14
	1/18	B	652	2.71	8.4	0.90			
	3/8	HTT	110	3.75	149.04	0.00			
Hg	1/18	H	**186**	**3**.45	− **6.6**	**0**.00			
	1/18	T	178	3.46	− 13.8	0.00	**H**	**B**	6
	1/18	B	180	3.49	− 19.0	0.27			
	3/8	HTT	124	3.60	489.70	0.00			

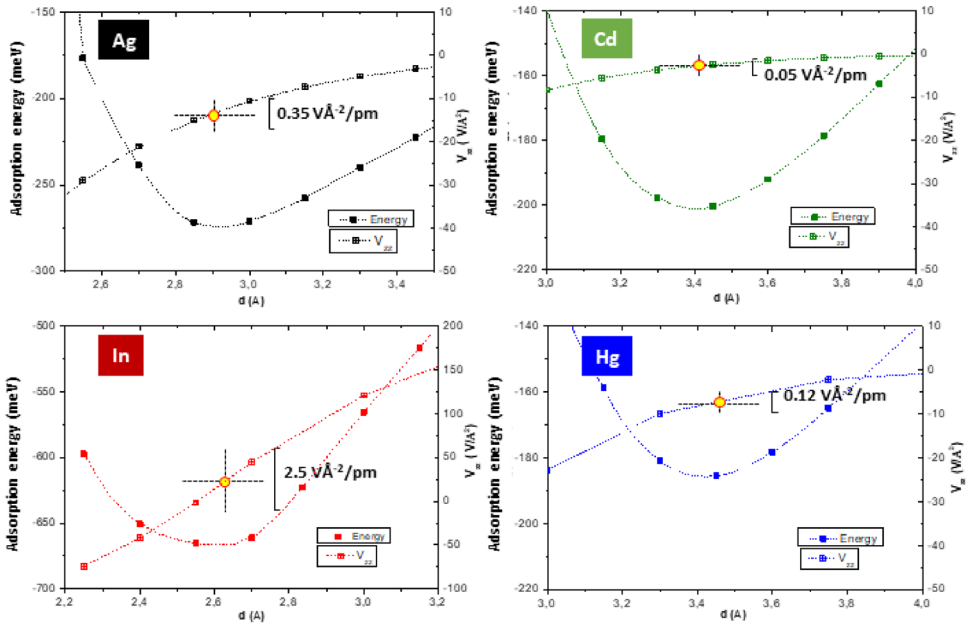

Fig. 4 V_{zz} at the adatom site and adsorption energy as a function of distance d for the most stable site: Ag (in a T site), Cd (in a H site), In (H) and Hg (H). The sensitivity of V_{zz} to the distance d, in the vicinity of the equilibrium position, is represented by a cross: the horizontal line has a length of $\Delta d = 20$ pm, i.e. of the order of the d steps used in the calculations; the vertical line has a length ΔV_{zz} corresponding to a $\Delta d = 20$ pm around the equilibrium position; the value of $\Delta V_{zz}/\Delta d$ is also given in units of V Å^{-2}/pm

dominated by contributions from the neighbouring metal atoms (in the isolated adatom regime, this contribution is negligible), masking the effects of the interaction with the graphene lattice.

Finally, we discuss how the calculated EFG parameters, which strongly depend on the local charge distribution, can be used in an experimental setting to study the binding and spatial configurations of adatoms on graphene. This involves comparing the EFG values calculated for possible configurations to those measured experimentally using hyperfine techniques.

Perturbed angular correlation (PAC) spectroscopy is a particularly suited technique to measure the EFG parameters. In order to illustrate what kind of information can

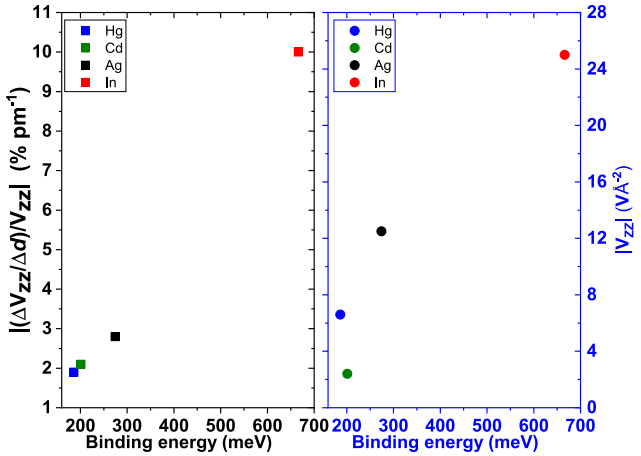

Fig. 5 Relative variation of V_{zz} ($|(\Delta V_{zz}/\Delta d)/V_{zz}^{eq}|$) in the vicinity of the equilibrium position, and absolute value of V_{zz}, as a function of binding energy, for Ag, Cd, In and Hg adatoms, in the most stale position of the isolated regime ($\theta = 1/18$)

be obtained from PAC experiments on atomic adsorption on graphene, we take the case of In, for which the EFG shows the highest sensitivity among the elements considered here. As an isolated adatom, In exhibits a migration barrier (ΔE_{hop} along H$\longleftrightarrow$B paths) of ~ 14 MeV which corresponds to a threshold temperature for diffusion of the order of 5 K. This value was estimated using an Arrhenius model for thermally activated diffusion: $\Lambda = \nu_0 e^{-\frac{E_d}{k_B T}}$, where Λ is the rate of thermally activated jumps, ν is the attempt frequency (which we take as $\nu_0 = 10^{12}\,s^{-1}$, of the order of the lattice vibrations), k_B the Boltzmann constant and T the temperature. We can then estimate the temperature regime associated with jumps between neighbouring sites within a certain time scale. For $\Delta E_{hop} = 14$ MeV, the temperature associated with 1 jump between neighbouring H sites within 1 min (60 s) window is 5 K.

In an experimental scenario, this implies that if In atoms are randomly deposited on graphene at liquid He temperatures, the mobility will be sufficiently low to allow to study In adatoms in their most stable high-symmetry site in an ideal (defect-free) graphene surface (H sites, based on the calculations presented here). At higher temperatures, with increasing mobility on the graphene surface, the adatoms would likely diffuse and become trapped in defective regions (e.g. graphene edges, Stone Wales defects, vacancies, grain boundaries) [27–29].

For PAC experiments on In, the decay of ^{117}Cd to the 315 keV excited state of ^{117}In through the 660 keV intermediate state (where the PAC measurement takes place) with spin of $3/2^-$ and 53.6 ns half-life is well established [30]. PAC is a time differential statistical measurement where the observable is the decay histogram of two consecutive γ-rays in coincidence. Taking into account the half-life of the mentioned probing state, no more than 400 ns (approximately 8 half-lives) can be resolved with enough statistics. Therefore, we estimate a limit such that half a period of the characteristic PAC perturbation function can still be resolved, i.e. 400/2 ns, leading to a minimum value of V_{zz} to be experimentally determined of 1.8 V/Å^2, with an uncertainty of about 2 % estimated from the uncertainty associated with the quadrupole moment. This implies that based on PAC measurements of V_{zz}, it would be possible to distinguish the two

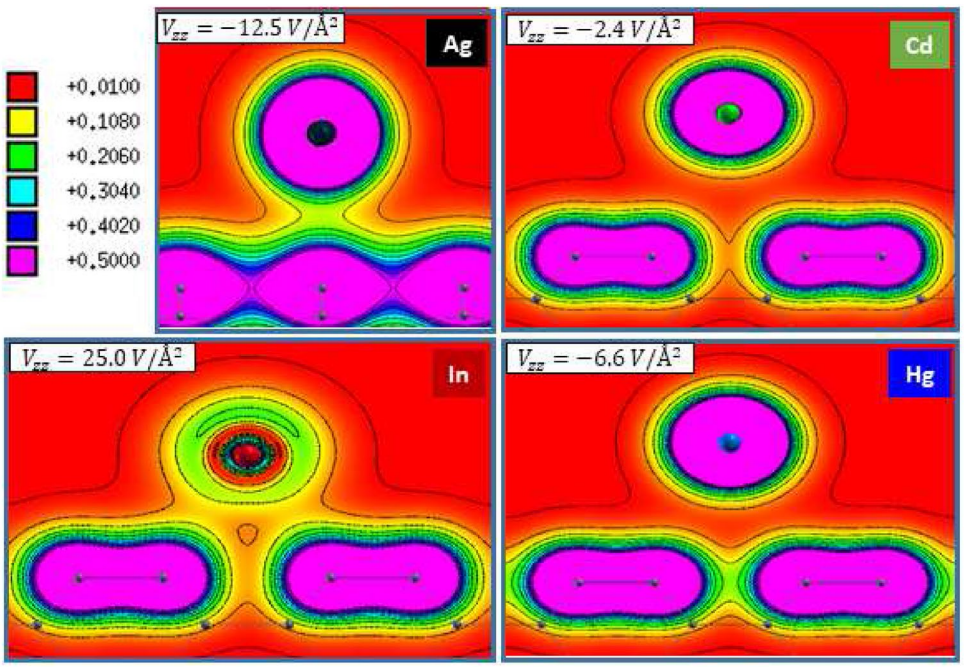

Fig. 6 Charge density (in units of e/Å^3) of the graphene–adatom system for the stable site and equilibrium distance of each adatom element: Ag (in a T site), Cd (in a H site), In (H) and Hg (H). The respective calculated V_{zz} is given in the inset. The orbital overlap decreases from In to Ag and then to Hg and Cd. As discussed in the text, the orbital overlap (charge sharing) is closely related to the binding strength and the EFG parameters

main regimes of In adatom concentration on graphene, i.e. between isolated In adatoms ($\theta = 1/18$) with $V_{zz} = 25\,\mathrm{V/Å^2}$ and the HTT monolayer ($\theta = 3/8$) $V_{zz} = 149\,\mathrm{V/Å^2}$.

Furthermore, in the isolated adatom regime, an experimental measurement would allow to identify which high-symmetry sites are occupied by In adatoms on graphene, and determine the adatom–graphene distance with high (sub-Å) precision (Table 1). Although according to the calculations presented here, for In adatoms on free standing graphene, the equilibrium configuration is that of isolated In adatoms on H sites, other configurations may be populated under the effect of additional parameters, such as an underlying substrate or applied fields.

Similar considerations could be done, for example, for Ag, although in that case, the T site was predicted to be the equilibrium site. Upon random deposition of sub-monolayer amounts of Ag at a sufficiently low temperature, the isolated state would, in principle, be observed. For higher concentrations, and with increasing temperature (thus increasing the mobility of the Ag adatoms), the monolayer configuration and its associated higher V_{zz} could eventually be observed.

Although the calculations presented here suggest that the dilute configuration is more stable than monolayer configurations, if we increase the concentration of adatoms segregation should occur. Moreover, shifts of the Fermi level due to defects or specific substrates may affect the electrostatic interaction between the adatoms and thereby stabilize monolayer configurations. Such experiments can be performed, for example, using the ASPIC setup at the ISOLDE facility at CERN [19], where adatoms can be deposited at low temperature, down to liquid He, and PAC measurements can be performed in situ as a function of temperature. While ASPIC has been previously used to investigate structural and magnetic properties of metal surfaces (e.g. Ni and Pd) [19], the calculations presented here show the potential of hyperfine techniques in the context of adatoms on graphene and on two-dimensional materials in general, by extension.

One of the advantages of this approach is that it allows to locally probe the adatom without affecting it, i.e. avoiding the influence of external probes, such as the tip of a scanning probe microscope or the intense electron beam of a transmission electron microscope. Additionally, a PAC spectrum can be measured with as little as 5^{10} probe atoms, corresponding to a coverage of 0.01% for a typical $5 \times 5\,\mathrm{mm^2}$ sample, i.e. the approach can be applied down to extreme levels of adatom dilution. Moreover, measurements are compatible with applied electric or magnetic fields [19].

Also very important, our calculations strongly indicate that the amount of information that can be addressed via the EFG parameters (sensitivity of the V_{zz} to changes in the atomic configuration) increases with the stability (binding energy), i.e. that the more robust the graphene–adatom system, the more prone it is to be studied using this approach.

In future studies, it would be interesting to extend these calculations to, for example, transition elements such as 3d transition metals or 4f rare earths. Not only can these elements be expected to exhibit even higher binding energies than In (e.g. in excess of 1 eV for Fe, Co and Ti [5]), and therefore even higher sensitivity of the EFG to structural observables, magnetic properties (e.g. local moment, magnetic order, etc.) could also be addressed via the magnetic hyperfine interaction.

4 Conclusions

For In, Ag, Cd and Hg, the isolated adatom regime is predicted to be the equilibrium configuration, which is more stable than the continuous monolayer configuration. In the isolated adatoms regime, the equilibrium site for Cd, In and Hg is found to be the H site; for Ag the T site.

The binding energy associated with the equilibrium configuration varies significantly among the elements considered here, from 110 MeV for a continuous In monolayer, to 666 MeV for isolated in adatoms.

In the most stable positions in the isolated adatom regime, a close relation was found between the binding stability (binding energy) and the sensitivity of the V_{zz} parameter. We interpret this relation as due to the shared origin of the graphene–adatom binding and the associated EFG at the adatom site: the orbital overlap (charge sharing) between the single adatom and the graphene layer and the associated asymmetry of the outer electron shells along the binding direction. Based on this relation, we propose that the V_{zz} parameter, which can be measured using hyperfine techniques, can be used in an experimental setting to probe the stability of atomic adsorption.

Furthermore, the EFG is found to be sensitive to the local atomic structure, distinguishing isolated from monolayer configurations, and for some cases, allowing to identify the high-symmetry site occupied by the adatoms and even monitor small variations in graphene–adatom distance with sub-Å precision. In particular, our calculations indicate that the level of detail that can be addressed via the EFG parameters (e.g. positional precision) increases with the stability (binding energy). In other words, the more stable graphene–adatom system (i.e. more relevant in a application scenario), the more it lends itself to be studied using hyperfine techniques.

Future studies could extend these calculations to other two-dimensional materials and other types of adatoms. For example, transition elements typically have high binding energies and therefore should exhibit a high sensitivity of the EFG to structural observables. Moreover, their magnetic

properties could also be addressed via the magnetic hyperfine interaction.

In addition to the ability to probe multiple adatom properties and phenomena (e.g. structural and magnetic), an experimental approach based on hyperfine techniques is generally compatible with ultra-high vacuum (typically necessary when studying surfaces, to minimize contamination), low temperature (typically necessary when studying isolated adatoms, due to their high surface mobility), and applied electric or magnetic fields (often used to investigate both basic and functional properties).

Acknowledgements This work was funded by the Portuguese Foundation for Science and Technology (FCT) (CERN-FIS-NUC-0004-2015, CERN-FIS-PAR-0005-2017, CERN/FIS-TEC/0003/2019, SFRH/BPD/82059/2011, SFRH/BD/93336/2013 and SFRH/BD/84743/2012), by CICECO-Aveiro Institute of Materials (UIDB/50011/2020 and UIDP/50011/2020)—FCT Ref. (UID/CTM/50011/2013), by the Scientific Research Flanders (G.0983.15) and the KU Leuven BOF (*CREA*/14/013 and *STRT*/14/002).

Data availability statement The data that support the findings of this study are available from the corresponding author upon reasonable request.

Declaration

Conflict of interest The authors declare that they have no conflict of interest.

References

1. K.S. Novoselov, A.K. Geim, S.V. Morozov, D. Jiang, Y. Zhang, S.V. Dubonos, I.V. Grigorieva, Science **306**(5696), 666–669 (2004)
2. A.K. Geim, K.S. Novoselov, Nat. Mater. **6**, 183–191 (2007)
3. N.M.R. Peres, Europhys. News **40**(3), 17–20 (2009)
4. K.T. Chan, J.B. Neaton, M.L. Cohen, Phys. Rev. B **77**, 235430 (2008)
5. H. Sevinçli, M. Topsakal, E. Durgun, S. Ciraci, Phys. Rev. B **77**, 195434 (2008)
6. A.V. Krasheninnikov, P.O. Lehtinen, A.S. Foster, P. Pyykkö, Phys. Rev. Lett. **102**, 126807 (2009)
7. R. Zan, U. Bangert, Q. Ramasse, K.S. Novoselov, Nano Lett. **11**(3), 1087–1092 (2011)
8. M. Vojta, L. Fritz, R. Bulla, Europhys. Lett. **90**(2), 27006 (2010)
9. V.W. Brar, R. Decker, H.-M. Solowan, Y. Wang, L. Maserati, K.T. Chan, H. Lee, Ç.O. Girit, A. Zettl, S.G. Louie, M.L. Cohen, M.F. Crommie, Nat. Phys. **7**, 43–47 (2011)
10. C. Gong, A.W. Robertson, K. He, C. Ford, A.A.R. Watt, J.H. Warner, Dalton Trans. **43**, 7442–7448 (2014)
11. S.C. Katrin Koch, *Analysis of an Electric-Field Gradient (EFG): the EFG-switch in LAPW2*. 2006
12. A. Lopes, *Local probe studies on lattice distortions and electronic correlations in CMR Manganites*. Aveiro University, 2006
13. K. Koch, *Crystal structure, electron density and chemical bonding in inorganic compounds studied by the Electric Field Gradient*. University of Dresden, 2009
14. S. Dey, C. Dey, S. Saha, Intermetallics **84**, 112–120 (2017)
15. D. Rettenwander, P. Blaha, R. Laskowski, K. Schwarz, P. Bottke, M. Wilkening, C.A. Geiger, G. Amthauer, Dft study of the role of al3+ in the fast ion-conductor li7-3 x al3+ x la3zr2o12 garnet. Chem. Mater. **26**(8), 2617–2623 (2014)
16. D. Torumba, V. Vanhoof, M. Rots, S. Cottenier, Phys. Rev. B **74**(1), 014409 (2006)
17. A. Fenta, C.O. Amorim, J. Gonçalves, N.M. Fortunato, M.B. Barbosa, J.P. Araujo, M. Houssa, S. Cottenier, M.J. Van Bael, J. Correia, *et al.*, *J. Phys. Mater.*, 2020
18. http://isolde.web.cern.ch/
19. K. Potzger, T.E. Mølholt, A.S. Fenta, L.M.C. Pereira, J. Phys. G: Nucl. Part. Phys. **44**(6), 064001 (2017)
20. http://susi.theochem.tu.ac.at.
21. S. Cottenier et al., Density functional theory and the family of (l) APW-methods: a step-by-step introduction. Instituut voor Kern-en Stralingsfysica, KU Leuven, Belgium **4**, 41 (2002)
22. K. Schwarz, P. Blaha, Comput. Mater. Sci. **28**(2), 259–273 (2003)
23. K. Schwarz, P. Blaha, G.K. Madsen, Comput. Phys. Commun. **147**(1–2), 71–76 (2002)
24. G. Giovannetti, P.A. Khomyakov, G. Brocks, V.M. Karpan, J. van den Brink, P.J. Kelly, Phys. Rev. Lett. **101**, 026803 (2008)
25. J.P. Perdew, K. Burke, M. Ernzerhof, Phys. Rev. Lett. **77**, 3865–3868 (1996)
26. S. Grimme, J. Antony, S. Ehrlich, H. Krieg, J. Chem. Phys. **132**(15), 154104–154104 (2010)
27. T.P. Hardcastle, C.R. Seabourne, R. Zan, R.M.D. Brydson, U. Bangert, Q.M. Ramasse, K.S. Novoselov, A.J. Scott, Phys. Rev. B **87**, 195430 (2013)
28. Q. Zhou, Y. Tang, C. Wang, Z. Fu, H. Zhang, Comput. Mater. Sci. **81**, 348–352 (2014)
29. Q. Zhou, Z. Fu, Y. Tang, H. Zhang, C. Wang, Phys. E **60**, 133–138 (2014)
30. A. Burchard, M. Deicher, V. N. Fedoseyev, D. Forkel-Wirth, R. Magerle, V. I. Mishin, D. Steiner, A. Stötzler, R. Weissenborn, T. Wichert, and ISOLDE Collaboration *Hyperfine Interact.*, vol. 120, pp. 389–395, 1999